Chemical Geology 495 (2018) 76–89

Contents lists available at ScienceDirect

Chemical Geology

journal homepage: www.elsevier.com/locate/chemgeo

Oxygen isotope fractionation during smithsonite formation from aqueous solutions

A. Füger[a,b,*], M. Méheut[c], V. Mavromatis[b,c], A. Leis[a], M. Dietzel[b]

[a] JR-AquaConSol GmbH, Steyrergasse 21, 8010 Graz, Austria
[b] Institute of Applied Geosciences, Graz University of Technology, Rechbauerstraße 12, 8010 Graz, Austria
[c] Géosciences Environnement Toulouse (GET), CNRS, UMR 5563, Observatoire Midi-Pyrénées, 14 Avenue Edouard Belin, 31400 Toulouse, France

ARTICLE INFO

Editor: E.B Michael

Keywords:
Smithsonite
Zinc carbonate
Oxygen isotope fractionation
Ab-initio calculation

ABSTRACT

Oxygen isotope fractionation between carbonate minerals and water is used as an environmental proxy to estimate mineral formation temperatures or isotopic composition of precipitating fluids. To date no experimental data on the oxygen isotope fractionation factor between smithsonite ($ZnCO_3$) and water, $\alpha(^{18}O)_{smithsonite\text{-}water} = (^{18}O/^{16}O)_{smithsonite} / (^{18}O/^{16}O)_{water}$, exist. Therefore, in the present study experimental work on smithsonite synthesis in the temperature range between 25 and 80 °C is coupled with ab-initio based theoretical calculations.

Laboratory precipitation experiments took place in titanium reactors at elevated pCO_2 (~10 atm) in order to induce the formation of smithsonite from hydrozincite ($Zn_5(CO_3)_2(OH)_6$), which is the precursor phase initially formed at 25 °C and low pCO_2 (pH ~ 6.8). The constant $\alpha(^{18}O)_{smithsonite\text{-}water} = (1000 + \delta^{18}O_{smithonite}) / (1000 + \delta^{18}O_{water})$ value reached at a reaction time ≥ 10,000 min (7 days) suggests near equilibrium conditions. Based on the experimentally obtained temperature relation of $\alpha(^{18}O)_{smithsonite\text{-}water}$ at 25, 40, 60, and 80 °C the integrated equation can be linearly described by the function:

$$10^3 \ln\alpha(^{18}O)_{smithsonite-water} = (2.79*10^6/T^2 - 0.95) \pm (0.06*10^6/T^2 + 0.60)$$

where the temperature is in Kelvin. The ab initio calculations suggest that this relation can be described in the temperature range from 0 to 100 °C as:

$$10^3 \ln\alpha_{smithsonite-liquid\ water} = (3.21*10^6/T^2 - 3.63) \pm (0.025*10^6/T^2 + 0.90)$$

The $\alpha(^{18}O)_{smithsonite\text{-}water}$ values from the experimental approach fit within error to the theoretical relationship from the literature and the above ab initio calculations. Difference in slope between the experiment and theoretical obtained equation likely reflects modeling inaccuracies, whereas kinetic effects cannot be completely ruled out in the experimental approach.

The obtained $\alpha(^{18}O)_{smithsonite\text{-}water}$ values match with the general sequence of $Zn^{2+} < Fe^{2+} < Mn^{2+} < Ca^{2+}$ for mono-cation trigonal Me-carbonate minerals suggesting incorporation of lighter oxygen isotopes in the carbonate mineral at increasing cation radius as indicated from thermodynamic considerations. Potential applications of oxygen isotope fractionation during smithsonite formation for natural aqueous surroundings are discussed.

1. Introduction

Zinc carbonate minerals are typically formed within the oxidation zone of zinc bearing ore bodies (Anthony et al., 2003). Two zinc carbonate minerals are known, smithsonite ($ZnCO_3$) and hydrozincite ($Zn_5(CO_3)_2(OH)_6$). Hydrozincite can be readily synthesized in the laboratory, whereas smithsonite synthesis is comparatively more complicated (Jambor, 1964; Bouchard and Smith, 2001; Zhu et al., 2001). Until now no experimental data exist for the oxygen isotope fractionation between smithsonite and water ($\alpha_{smithsonite\text{-}water} = (^{18}O/^{16}O)_{smithsonite} / (^{18}O/^{16}O)_{water}$) and its temperature dependence. This lack of data is likely caused by the seldom occurrence of the

* Corresponding author at: JR-AquaConSol GmbH, Steyrergasse 21, 8010 Graz, Austria.
E-mail address: Anja.Fueger@jr-aquaconsol.at (A. Füger).

https://doi.org/10.1016/j.chemgeo.2018.08.005
Received 16 March 2018; Received in revised form 31 July 2018; Accepted 3 August 2018
Available online 05 August 2018

physicochemical conditions required for smithsonite formation in Earth's surface environments and the competitive precipitation of hydrozincite. The formation conditions for smithsonite versus hydrozincite are strongly controlled by the partial pressure of CO_2. Under Earth's atmospheric conditions (CO_2 partial pressure of about $10^{-3.5}$ atm) hydrozincite is the stable zinc carbonate phase. If the partial pressure of CO_2 increases smithsonite formation is favored, depending in particular on pH and on dissolved inorganic carbon (DIC refers to $CO_{2(aq)}$, H_2CO_3, HCO_3^-, and CO_3^{2-}) concentration (Alwan and Williams, 1979; Williams, 1990).

Since Urey's work in 1947 and from a large number of experimental (e.g. McCrea, 1950; O'Neil et al., 1969; Tarutani et al., 1969; McConnaughey, 1989; Kim and O'Neil, 1997; Kim et al., 2006; Dietzel et al., 2009; Mavromatis et al., 2012) and theoretical (e.g. Urey, 1947; Zheng, 1999; Watson, 2004; Schauble et al., 2006; Chacko and Deines, 2008; Zheng, 2011) studies thereafter, it is well established that oxygen isotopes fractionate strongly between carbonate minerals and the aqueous fluid from which they are formed. The respective isotope fractionation factor α, defined as the ratio of the abundance of the isotopomers ^{18}O and ^{16}O in the two phases, significantly depends on temperature (Urey, 1947; McCrea, 1950). Thus oxygen isotopes in carbonates provide an excellent tool to unravel formation temperature, providing that the isotopic composition of their parent solution is known or can be reasonably estimated. Typically the equilibrium oxygen isotope fractionation factor decreases as temperature increases (e.g. Hoefs, 2015). In order to use oxygen isotope fractionation as geological thermometer besides equilibrium fractionation kinetic effects also have to be evaluated (e.g. Dietzel et al., 2009). The kinetics of isotopic exchange and the reaction mechanisms between carbonate minerals and water, as well as between the DIC species and water have to be considered (e.g. McCrea, 1950; Beck et al., 2005; Kim et al., 2006) as each species has a distinct oxygen isotope fractionation compared to water (McCrea, 1950).

Already in 1953, Epstein and co-workers documented oxygen isotope fractionation of various alkaline earth carbonates to differ up to several per mil. After the study of McCrea (1950) on temperature variation of the fractionation of oxygen isotopes between dissolved inorganic carbon and water as well as between calcite and water, the isotopic compositions of a large variety of carbonate minerals such as strontianite and witherite (O'Neil et al., 1969), biogenic induced aragonite (Tarutani et al., 1969), siderite (Becker and Clayton, 1976; Carothers et al., 1988; van Dijk et al., 2017), inorganic aragonite (Zhou and Zheng, 2002, 2003; Kim et al., 2006) have been investigated. The oxygen isotope fractionation ($10^3 \ln\alpha_{carbonate\_mineral\text{-}water} \approx \Delta^{18}O_{carbonate\_mineral\text{-}water} = \delta^{18}O_{carbonate\_mineral} - \delta^{18}O_{water}$) among carbonate minerals varies from 23‰ for strontianite (Chacko and Deines, 2008) up to 32‰ for dolomite at 25 °C (Schmidt et al., 2005). Up to date, for smithsonite only theoretical studies on oxygen isotope fractionation exist (e.g. Zheng, 1999; Chacko and Deines, 2008).

Theoretical studies are based on the vibrational properties of the phases of interest. Accordingly, Chacko and Deines (2008) have computed the mineral-CO_2 fractionation for many carbonate minerals, including smithsonite, based on the experimentally measured vibrational properties of these phases. The mineral-liquid water fractionation (e.g. 32.18 ± 0.21‰ for smithsonite at 25 °C) is obtained accordingly by combining CO_2-H_2O experimental data (see Rosenbaum, 1997). However, Chacko and Deines (2008) base their work on several simplifying assumptions (see Deines, 2004) and rely on the quality of available experimental data, which can differ for two different minerals such as calcite and smithsonite (see the Methodology section of Chacko and Deines (2008) for further details). Another approach to assess the full vibrational properties of those phases, independently of any experiment, is based on the electronic structure modeling of minerals and molecules that was developed for mineral-water fractionation behaviors (e.g. Méheut et al., 2007). In the case of the electronic structure-based calculation, there are two principal sources of critical uncertainties: (1) the inevitable choice of an approximate exchange-correlation functional, at the foundation of the electronic structure calculation, induces errors on the harmonic vibrational properties. This corresponds at first order to an identical relative underestimation of all vibrational frequencies (e.g. around 5%). (2) The model does not include anharmonic effects for the water molecule. A new ab initio modeling for oxygen isotope fractionation is herein applied to yield theoretical $\alpha(^{18}O)_{smithsonite\text{-}vapour\_H2O}$ values, further combined with the experimental vapor-liquid fractionations of Horita and Wesolowski (1994) to obtain $\alpha(^{18}O)_{smithsonite\text{-}water}$. We provide this by an approach based on the electronic structure modeling of minerals and molecules with correction for the above mentioned uncertainties (e.g. Méheut et al., 2007). This approach is first validated on the well constrained case of the calcite-water equilibrium and then applied to smithsonite.

In the present study we experimentally determine the until now poorly constrained oxygen isotope fractionation between smithsonite and water as a function of temperature. The formation of smithsonite was induced by the transformation of hydrozincite between 25 and 80 °C. The experimental fractionation coefficients were assessed in comparison to the theoretical values generated in this study and from the literature. The obtained temperature-controlled oxygen isotope fractionation kinetics, reaction mechanisms and the implications to natural smithsonites and smithsonite forming environments are addressed.

2. Methods

2.1. Experimental setup

Smithsonite was synthesized at the temperature range 25 to 80 °C (± 0.5 °C) at 10 atm CO_2 pressure in either a PARR© non-stirred high-pressure titanium batch reactor (4601–4622 General Purpose Reactors), or a PARR© stirred high pressure titanium batch reactor (4560 Mini Reactors) both equipped with electrical heaters. An illustration of the experimental set-up used in this study can be seen in Fig. 1. The use of two different setups (with and without stirring) served as a control of the reproducibility of the obtained experimental results. The experimental solution was prepared by mixing 250 ml of two stock solutions, the first containing 0.2 M of $NaHCO_3$ (Carl Roth, ≥ 99.5%, p.a., ACS,

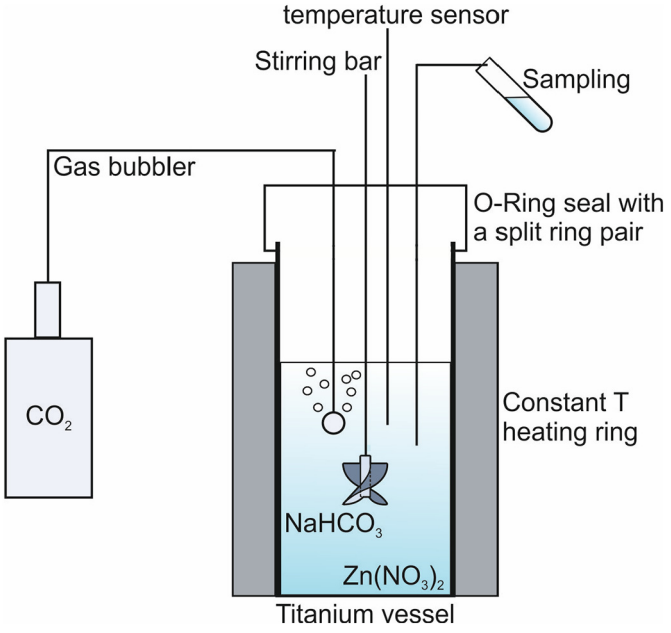

Fig. 1. Experimental set-up of the high pressure titanium batch reactor which was used for experiments with and without using the stirring bar.

ISO) and the second containing 0.04 M of $Zn(NO_3)_2$ (Merck, ≥ 98.5%, p.a.), in the reactor at ambient temperature. Owing to the high supersaturation of the reactive solution with respect to hydrozincite, this zinc hydroxide carbonate mineral (pH 6.83 ± 0.17) is formed instantaneously after the mixing of the two stock solutions at ambient conditions according to the overall reaction

$$5\ Zn^{2+} + 10\ HCO_3^- = Zn_5(CO_3)_2(OH)_{6\,(s)} + 8\ CO_2 + 2\ H_2O \quad (1)$$

After the mixing of the stock solutions the reactors were immediately sealed and pressurized at $pCO_2 \sim 10$ atm (within ~10 min after mixing). The low pH conditions (pH 5.4 ± 0.2), provoked by the prevailing elevated pCO_2, lead to the dissolution of hydrozincite and the subsequent formation of smithsonite according to the overall reaction

$$Zn_5(CO_3)_2(OH)_{6\,(s)} + 3\ CO_2 \rightarrow 5\ ZnCO_{3\,(s)} + 3\ H_2O. \quad (2)$$

In total 20 experiments were performed, with reaction times ranging from 465 to 72,620 min (about 8 h to 50 days) in order to follow the temporal evolution of smithsonite formation as well as its oxygen isotope composition. At the end of each experiment the reactor was quenched and subsequently the solution was separated from the precipitate using vacuum filtration and 0.1 µm filters (Millipore, cellulose acetate). Aliquots (1 ml) were sampled from the reactive solution in-situ for alkalinity and 10 ml aliquots for oxygen isotope analyses of the solution. Additional, an aliquot was acidified to a 2% HNO_3 matrix for analysis of Zn and Na concentrations using HNO_3 of suprapure grade (Roth ROTIPURAN®). The separated precipitates were thoroughly rinsed with MilliQ water three times to remove adsorbed Zn ions from the solid surface and subsequently dried at 40 °C for solid phase characterization.

2.2. Analytics

2.2.1. Solid characterization

The collected solids were analyzed using Attenuated Total Reflectance - Fourier Transform Infrared Spectroscopy (ATR-FTIR; Perkin Elmer Spektrum 100) equipped with a $ZnSeO_4$ crystal in the wavenumber range from 650 to 4000 cm^{-1}. X-ray powder diffraction (XRD) patterns of the precipitates were measured using a PANalytical X'Pert PRO diffractometer and Co-Kα-radiation (40 mA, 40 kV) over 50 min at a range from 4° to 85° and a scan speed of 0.03° min^{-1}. The mineral phases were quantified by Rietveld refinement using the PANalytical X'Pert HighScore Plus software with its associated PDF-2 database. Selected solids were imaged using a ZEISS DSM 982 Gemini scanning electron microscope (SEM) operating at 2 kV accelerating voltage.

2.2.2. Chemical analyses

Alkalinity of the reactive solutions was measured by potentiometric titration using 0.01 M HCl and a Schott TitroLine alpha plus titrator with an uncertainty of ± 2%. The pH of the same aliquots was measured using a WTW IDS pH-meter combined with a SenTix® 945 pH gel electrode with a glass shaft from WTW, calibrated against NIST standard buffers at pH = 4.01, 7.00 and 10.01 at 20 °C (analytical error: ± 0.03 pH units). Aqueous concentrations of Zn and Na were analyzed in acidified (2% HNO_3) aliquots by inductively coupled plasma optical emission spectroscopy using a Perkin Elmer Optima 8300 DV ICP-OES. A range of SPS-SW2 Batch 130 and NIST 1640a standards were measured at the beginning and end of a sample series and had an analytical error (2 s, 3 replicates) of ± 3% for all elements relative to the standards.

2.2.3. Geochemical modeling

Aqueous speciation of the reactive solutions, ion activities and saturation degree (Ω = IAP/solubility constant) of the reactive solutions with respect to smithsonite (see Table 1), hydrozincite, and zincite were calculated using PHREEQC software (Parkhurst and Appelo, 1999) together with its MINTEQ.V4 database as well as PHREEPLOT (Kinniburgh and Cooper, 2011) to establish a stability diagram of the Zn-CO_2-H_2O system.

2.2.4. Oxygen isotopic analyses

The most common way to analyze the oxygen isotope composition of solid carbonates is to use a modification of the original phosphoric acid reaction technique developed by McCrea (1950). The oxygen isotope composition of smithsonite ($\delta^{18}O_{smithsonite}$) was measured with a Gasbench II sample preparation device interfaced to a Thermo Finnigan DeltaplusXP a Finnigan GasBench II mass spectrometer using the common phosphoric acid method (Révész and Landwehr, 2002; Spötl and Vennemann, 2003; Paul and Skrzypek, 2007). To measure the oxygen isotope composition of the precipitates, aliquots of approximately 500 µg material were transferred into 10 ml glass vials and flushed with helium, using a gas flow of 100 ml/min to remove residual air from the sample vials. Phosphoric acid (99%) added a couple of drops into each sample vial; the produced CO_2 is manually transferred onto a Gas Chromatography column using a flow rate of 1.5 ml/min at 72 °C, where the CO_2 was chromatographically separated from other components of the gas sample. The analytical error of the $\delta^{18}O_{smithsonite}$ values, reported relative to the VPDB standard, was ± 0.1%.The oxygen isotope ratios of the final reactive solution were measured in 0.3 ml subsamples with the classical CO_2–H_2O equilibration method (Epstein and Mayeda, 1953) using a dual inlet Thermo Finnigan Deltaplus mass spectrometer coupled to an automated preparation unit adopted from Horita et al. (1989). The measurements were carried out at 24 °C with a precision < 0.1‰. All $\delta^{18}O_{water}$ values are reported relative to VSMOW (Vienna Standard Mean Ocean Water), calculated using equations by Coplen et al. (1983).

The measured $\delta^{18}O_{smithsonite}$ values were expressed on the VPDB scale using the normalization protocol IUPAC developed by Kim et al. (2015) coupled with the phosphoric acid fractionation factor for smithsonite reported by Gilg et al. (2003) for the reference materials NBS 19 and NBS 18 at 72 °C. The $\delta^{18}O_{smithsonite}$ values were converted to the VSMOW scale using the expression

$$\delta^{18}O_{VSMOW} = 30.92 + 1.03092 * \delta^{18}O_{VPDB} \quad (3)$$

The oxygen isotopic fractionation factor between smithsonite and water was calculated using the equation

$$\alpha_{smithsonite-water} = (1000 + \delta^{18}O_{smithsonite})/(1000 + \delta^{18}O_{water}) \quad (4)$$

2.3. Ab initio calculations of mineral-water vapor oxygen isotopic fractionation factors at the harmonic level

The equilibrium mineral-water vapor fractionation of oxygen isotopes is obtained by combining the β-factors of both phases. The isotopic fractionation factor of an element between two phases *A* and *B*, is defined as the overall ratio of isotopes *Y* and *Y** in the phase *A* as compared with the same ratio in *B*. Both phases *A* and *B* contain two isotopic forms *Y* and *Y**. *Y** corresponds to the least abundant isotope. The β-factor corresponds to the isotopic fractionation factor of *Y* between the phase *A* and a perfect gas of *Y* atoms. This quantity can be computed, with the harmonic approximation, from the vibrational frequencies of the phase of interest (Bigeleisen and Mayer, 1947). The β-factor of water vapor in the harmonic approximation is computed following Méheut et al. (2007). The β-factors of calcite and smithsonite are computed from their phonon frequencies with Eqs. (8) and (16) of Méheut et al. (2007). The phonon frequencies are computed from first-principles using density functional theory (DFT) (Hohenberg and Kohn, 1964; Kohn and Sham, 1965). The calculation was based on the exchange-correlation functional of Perdew, Burke and Ernzerhof (PBE) (Perdew et al., 1996), a plane-wave basis set, and atomic pseudopotentials as implemented in the Quantum Espresso package. The pseudopotentials used for O and H are described in the

Table 1
Temperature, pH, duration, added $NaHCO_3$ and $Zn(NO_3)_2$ of the experimental solution. $\delta^{18}O$ values of the precipitates relative to Vienna Standard Mean Ocean Water (VSMOW). $10^3\ln\alpha(^{18}O)_{precipitate-water}$: oxygen isotopic fractionation between the precipitate and water ($\delta^{18}O_{water} = -9.58 \pm 0.33$, ‰; VSMOW).

No.	T (°C)	pH	t (min)	Added $NaHCO_3$ (mM)	Added $Zn(NO_3)_2$ (mM)	$\delta^{18}O_{precipitate}$	$10^3\ln\alpha(^{18}O)^*_{precipitate-water}$	$\Omega_{precipitate}$
Precursor phase (hydrozincite)								
T25_0[a]	25	6.83	0	199.8	40.9	22.75	32.11	$10^{7.01}$
Smithsonite (non-stirring)								
T25_1.1	25	5.31	465	228.7	43.5	19.43	28.97	13.49
T25_1.2	25	5.42	1160	199.5	44.2	20.11	29.64	26.30
T25_1.3	25	5.35	1410	249.5	43.2	20.49	29.95	13.80
T25_1.4	25	5.46	4485	199.6	42.1	21.24	30.69	8.32
T25_1.5	25	5.41	10,050	201.4	42.8	20.77	30.32	3.80
T25_1.6	25	5.40	20,150	199.4	43.2	20.74	30.26	3.24
T25_1.7	25	5.48	30,270	202.0	42.8	20.87	30.36	2.09
T25_1.8	25	5.39	58,790	201.2	43.0	21.05	30.41	1.74
T25_1.9	25	5.38	72,620	207.7	44.2	21.06	30.50	1.05
T40_1	40	5.32	24,240	98.1	21.8	17.93	27.35	3.89
T40_2	40	5.54	4125	199.8	39.1	18.09	27.28	6.17
T60_1	60	5.50	18,815	100.2	20.0	14.41	23.79	7.24
T60_2	60	5.06	26,930	103.0	21.1	14.23	24.32	2.14
T80	80	5.48	10,035	100.0	21.0	12.22	21.38	10.96
Smithsonite (stirring)								
T25s_1.1	25	5.61	490	226.4	36.9	21.06	30.44	57.54
T25s_1.2	25	5.51	930	188.5	39.8	20.6	30.02	44.67
T25s_1.3	25	5.45	1345	170.1	39.8	19.99	29.51	39.81
T25s_1.4	25	5.40	4490	179.0	38.5	20.14	29.64	28.18
T25s_1.5	25	5.38	10,170	166.4	39.5	19.87	29.34	26.92
T25s_1.6	25	5.43	20,040	202.1	39.9	19.84	29.35	3.80

s = precipitation of smithsonite by using a stirred reactor.
[a] hydrozincite precipitated at the initial stage of the experiments at 25 °C.

electronic annexes of Méheut et al. (2007). The pseudopotentials used for Ca and Zn were taken from the PSlibrary (Dal, 2014). For the C pseudopotential, we used the $1s^2$, $2s^2$, $2p^2$ configuration, with core radius 1.23, 1.23 a. u., respectively.

Computational details for water vapor are the same as in Méheut et al. (2007). For calcite and smithsonite, electronic wave-functions are expanded in plane-waves up to an energy cutoff $\varepsilon_{cut} = 80$ Ry and the charge density cut-off is set to 4 ε_{cut}. The electronic structure integration is performed by sampling the first Brillouin zone with a $3 \times 3 \times 3$ k-points grid according to the Monkhorst-Pack scheme (Monkhorst and Pack, 1976).

Phonon frequencies are computed using linear response theory (Baroni et al., 2001) with the Quantum Espresso package (Giannozzi et al., 2009). Interatomic force-constants are obtained from the dynamical matrices computed exactly (within DFT) on a $3 \times 3 \times 3$ grid of q-vectors.

Long-range effects are taken into account by computing Born effective-charges and static dielectric constants (Baroni et al., 2001). Dynamical matrices and thus phonon frequencies can then be obtained in any point of the reciprocal space by Fourier-interpolation of the force constants. For smithsonite, the β-factor is converged with a 6x6x6 interpolation grid.

3. Results

3.1. Mineralogy of the precipitates

The collected FT-IR spectra of synthetic smithsonite compared to those of the intermediate reaction product hydrozincite can be seen in Fig. 2A. Smithsonite exhibits vibration bands at 742 (carbonate ν_4 in phase bending mode), 841 (carbonate ν_2 bending mode), 1078 (carbonate ν_1 stretching mode) and 1378 cm^{-1} (carbonate ν_3 vibrational mode) in agreement with Hales and Frost (2007). Note here that it is generally expected that the ν_2 bending mode of carbonates lay within the frequency range from 890 to 850 cm^{-1} (Farmer, 1974), a range of values that is somewhat higher compared to those of our study (Fig. 2A). The occurrence however of the ν_2 band at 841 cm^{-1} – observed in this study – is in excellent agreement with that reported by Hales and Frost (2007) for smithsonite. The infrared spectrum of hydrozincite shows additional infrared bands to smithsonite at 949 cm^{-1} and 3306 cm^{-1}, both attributed to hydroxide vibrations (Stoilova et al., 2002). The X-ray diffraction pattern of the precipitated solid is compared to a reference smithsonite spectrum in Fig. 2B, which suggests smithsonite to be the sole reaction product in all experiments performed at elevated CO_2 pressure.

From SEM imaging (Fig. 3A) it can be seen that the initially precipitated hydrozincite consists of nanosized spherical particles with < 1 µm in diameter that are similar in form to the hydrozincite shape documented earlier by Wahab et al. (2008), whereas in the final reaction product no hydrozincite is present as it is confirmed by both XRD and SEM analyses. In addition Fig. 3 illustrates changes in the texture of the growing smithsonite crystals throughout the experimental runs and for distinct formation temperatures. For instance, in experiments at 25 °C, the size of crystal aggregates increased with reaction time. Smithsonite incubated for 1160 and 20,150 min (Fig. 3B and C) comprised of crystal aggregates with a diameter of 5 µm. At 30270 min reaction time the diameter of the crystal aggregates are about 10 µm (Fig. 3D), whereas at 72620 min reaction time the diameter of the crystal aggregates increased up to about 20 µm (Fig. 3F). The crystal aggregates of smithsonite consist of rhombohedral crystals with an edge length of about 1 µm. In contrast, at higher temperatures the edge length of the rhombohedral smithsonite crystals increased, but crystal aggregates are in the same dimension (Fig. 3G at 60 °C for 26,930 min).

3.2. Chemical composition of the reactive solution

The chemical composition of the reactive solution was used to calculate the temporal evolution of pH and supersaturation in respect to smithsonite. The pH of the reactive solution (see Fig. 4A) for the experiments using the non-stirring reactor is increasing between 465 and 1410 min with a maximum at about 1160 min, whereas the pH for the experiments using the stirring reactor decreased over the same time interval. The pH for both experiments - using the stirring and non-stirring reactor - is approaching a constant pH of 5.4 ± 0.05 with increasing reaction time. The supersaturation of the reactive solution in respect to

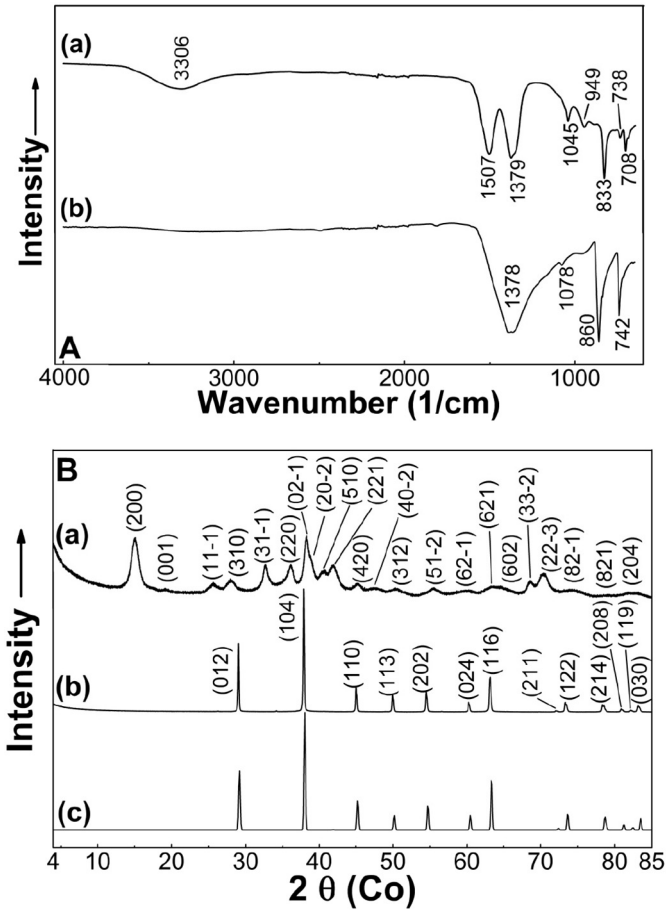

Fig. 2. (A) Typical FT-IR spectra of (a) precipitated hydrozincite (exp. T25_0) from the beginning of each experiment at ambient conditions at a reaction time of 1 min and (b) precipitated smithsonite from exp. T25_1.1 at 10 pCO2 (atm) and 25 °C at a reaction time of 480 min; and (B) Characteristic X-ray diffraction pattern of (a) precipitated hydrozincite (exp. T25_0) from the beginning of each experiment at ambient conditions at a reaction time of 1 min, (b) precipitated smithsonite from exp. T25_1.1 at 10 pCO2 (atm) and 25 °C at a reaction time of 480 min and (c) smithsonite (FIZ Karlsruhe, ICSD database; PDF-number: 01-083-1765 8-449).

smithsonite follows the evolution of pH, i.e. decreasing between 490 and 1345 min (Fig. 4B) for the experiments using the stirring reactor. In contrast, between 465 and 1410 min the $\Omega_{smithsonite}$ for the experiments using the non-stirring reactor show a maximum at about 1160 min. As with pH, the supersaturation of the reactive solution with respect to smithsonite reaches an approximately equal value in both experiments of $\Omega_{smithsonite} = 1.1 \pm 0.3$. The pH and the supersaturation state evolution indicates the approach of chemical equilibrium conditions for smithsonite and confirms the accuracy of solubility data from Schindler et al. (1969). The pH-induced $\Omega_{smithsonite}$ evolution is strongly based on the pH dependence of DIC species distribution. The pH difference in the non-stirring versus stirring reactive solutions can be likely explained by the delayed neutralization of the in CO_2 loaded solution due to hydrozincite transformation to smithsonite at non-stirring conditions.

3.3. Oxygen isotopic fractionation factor between smithsonite and solution at 25 °C

The temporal evolution of the oxygen isotope fractionation between carbonate precipitate and water has been studied in detail for experiments performed at 25 °C. The oxygen isotopic composition of the water used in our experiments was measured to be $\delta^{18}O_{water} = -9.58 \pm 0.33‰$ (VSMOW; $n = 20$). The temporal evolution of the $10^3 ln\alpha_{smithsonite\text{-}water}$ values is displayed in Fig. 5. The $10^3 ln\alpha_{smithsonite\text{-}water}$ value at ≥10,000 min (i.e. 7 days) of the experimental run time is about 30.5 ± 0.1‰ using the non-stirring reactor, whereas it is about 29.4 ± 0.1‰ in experiments conducted with the stirring reactor (Table 1). Note here, that the apparent $10^3 ln\alpha_{hydrozincite\text{-}water}$ value between hydrozincite and water is slightly higher (32.1 ± 0.1‰ at 25 °C; see Table 1) compared to that measured between smithsonite and water. Although the final $\alpha_{smithsonite\text{-}water}$ values are almost identical within the overall accuracy of the used experimental approach, the temporal evolution using the stirring and non-stirring reactor were significantly different at the beginning of the runs. The $10^3 ln\alpha_{smithsonite\text{-}water}$ values decrease by using the stirring reactor, whereas the experiments performed in the non-stirring reactor indicate an increase of $\alpha_{smithsonite\text{-}water}$ with time. These findings indicate that a synthesis duration of about 10,000 min (Fig. 5) is likely needed in the experimental runs to approach a constant isotopic fractionation between smithsonite and water at 25 °C, where also thermodynamic equilibrium is approached (see Fig. 4A and B). Accordingly, less time for approaching constant isotope composition can be expected for the experiments at elevated temperatures.

3.4. Oxygen isotopic fractionation factor between 25 and 80 °C

As a constant isotopic fractionation between smithsonite and water is reached at about 10,000 min for $T \geq 25$ °C the obtained $10^3 ln\alpha_{smithsonite\text{-}water}$ values at $t \geq 10{,}000$ min were used to obtain a T dependence of apparent oxygen isotope fractionation between smithsonite and water up to 80 °C (see Table 1; Fig. 6). The experimental findings indicate a strong negative temperature control on $10^3 ln\alpha_{smithsonite\text{-}water}$ according to the expression

$$10^3 ln\alpha_{smithsonite-water} = (2.79*10^6/T^2 - 0.95) \pm (0.06*10^6/T^2 + 0.60) \quad (5)$$

where high temperatures result in lower α values that can be attributed to near isotopic equilibrium conditions.

3.5. Theoretical calculations of calcite-water and smithsonite-water oxygen isotope fractionation at equilibrium

Cell parameters of calcite and smithsonite are obtained at zero pressure until the residual forces are $< 10^{-3}$ Ry/Å (Table 2). They are generally overestimated by around 1–2%, which is the usual trend with GGA PBE functional. A good agreement is observed between calculated frequencies and experimental ones (Table 3). Generally, the calculated frequencies underestimate experimental results by a few %, but the relative difference is varying depending on the modes. The ratio between calculated harmonic frequencies and corresponding experimental frequencies is discussed in detail in Appendix A. For calcite and smithsonite this ratio was found to be essentially identical for the two carbonate minerals, and equal to 0.957 ± 0.006, where the error stands for the standard error on this ratio. This is consistent with the results from Schauble et al. (2006) who concluded on the adequacy of a unique scale factor for several anhydrous carbonate minerals.

The mineral-water vapor fractionation factors, calculated from the raw ab initio-based harmonic frequencies, are given as a function of temperature in Table 4 and represented on Fig. A3. These calculations are affected by two errors of different origin. First, harmonic frequencies calculated within our approach underestimate experimental harmonic frequencies by a few percent. This underestimation was corrected by multiplying all mode frequencies of a given material by an identical scale factor, deduced from the comparison of experimental harmonic frequencies and calculated harmonic frequencies (see details in Appendix A). For water vapor, experimental harmonic frequencies are available, and can be compared to our calculation (see Table 1 of Méheut et al., 2007). The obtained scaling factor is 0.954 ± 0.003 (1SE) (see details in Appendix A). For calcite and smithsonite, however, the only available experimental frequencies are anharmonic.

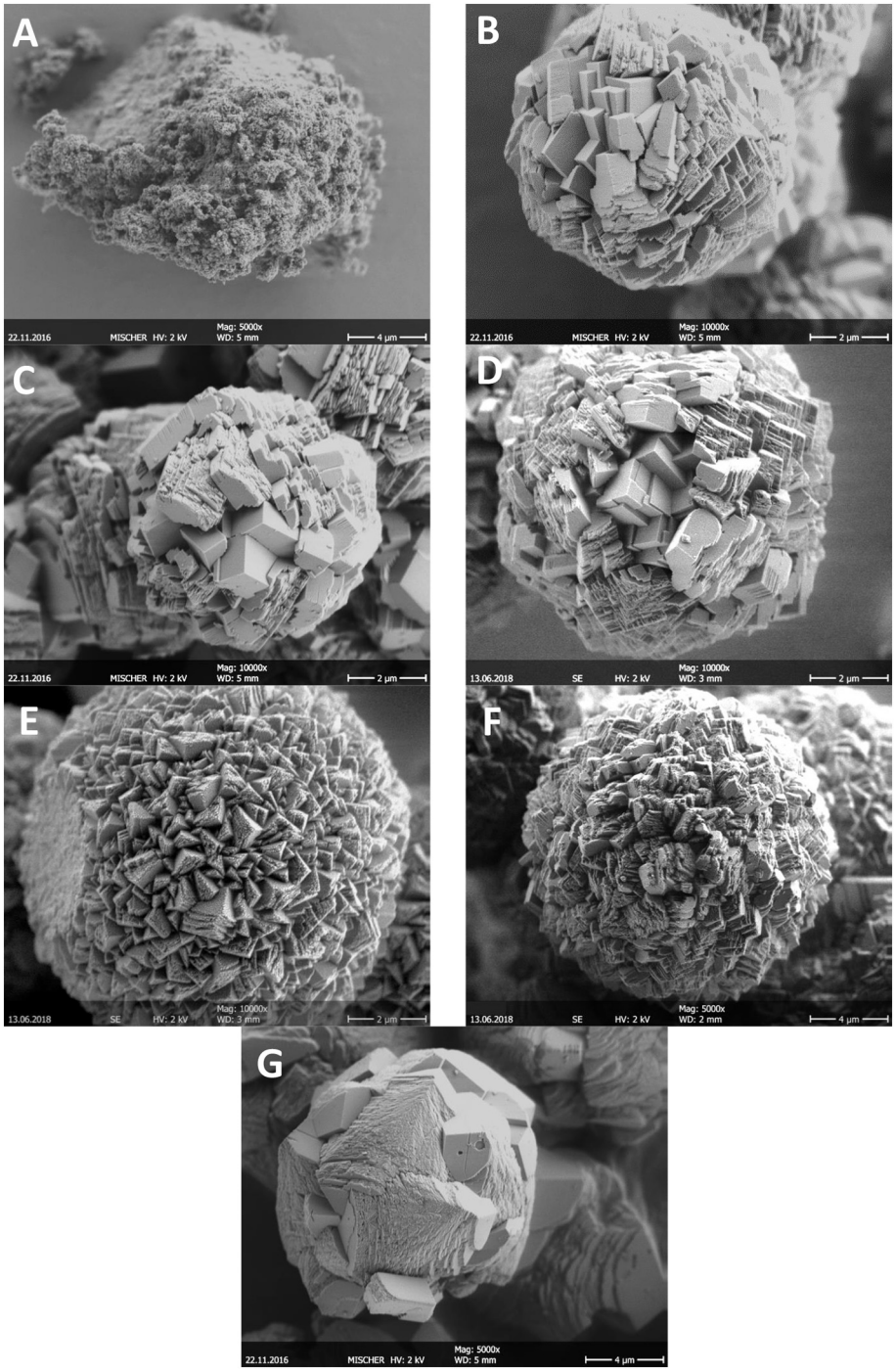

Fig. 3. Scanning electron microphotographs of precipitated (A) hydrozincite (characteristic transition phase precipitated at 25 °C in all experiments; exp. T25_0) and (B) typically precipitated smithsonite (exp. T25_1.2; pCO2 = 10 atm; 25 °C; 1160 min), (C) smithsonite (exp. T25_1.6; pCO2 = 10 atm and 25 °C at 20150 min reaction time), (D) smithsonite (exp. T25_1.7; pCO_2 = 10 atm; 25 °C; 30,270 min), (E) smithsonite (exp. T25_1.8; pCO_2 = 10 atm; 25 °C; 58,790 min), (F) smithsonite (exp. T25_1.9; pCO_2 = 10 atm; 25 °C; 72,620 min), and (G) smithsonite (exp. T60_2; pCO2 = 10 atm; 60 °C; 26,930 min).

Anharmonic effects in calcite and smithsonite are nevertheless expected to be small (see below), and we therefore used the experiment over calculation frequency ratio discussed above (0.957 ± 0.006) as our scaling factor.

Second, the expressions used for the β-factors (equation (11) of Méheut et al., 2007 for water vapor, equation (16) of Méheut et al., 2007 for the carbonates) are based on the harmonic approximation. For water vapor, Richet et al. (1977) proposed a simple correction for anharmonic effects based on experimental frequencies (equation 49 of Richet et al., 1977). We simply added this correction to our water vapor β-factor. For calcite and smithsonite, the vibrations were assumed to be harmonic, and therefore no anharmonic correction was applied. This situation – a gas treated anharmonically, and carbonates considered harmonic – has been discussed by Chacko and Deines (2008) study. Based on the estimation of anharmonic effects in calcite by Gillet et al. (1996) and Polyakov (1998), these authors concluded that these hypotheses may lead to an over- or underestimation by about 0.5‰ of gas-carbonate fractionation.

The corrected mineral-water vapor fractionation factors are given as a function of temperature in Table 4 and represented in Fig. A3. The

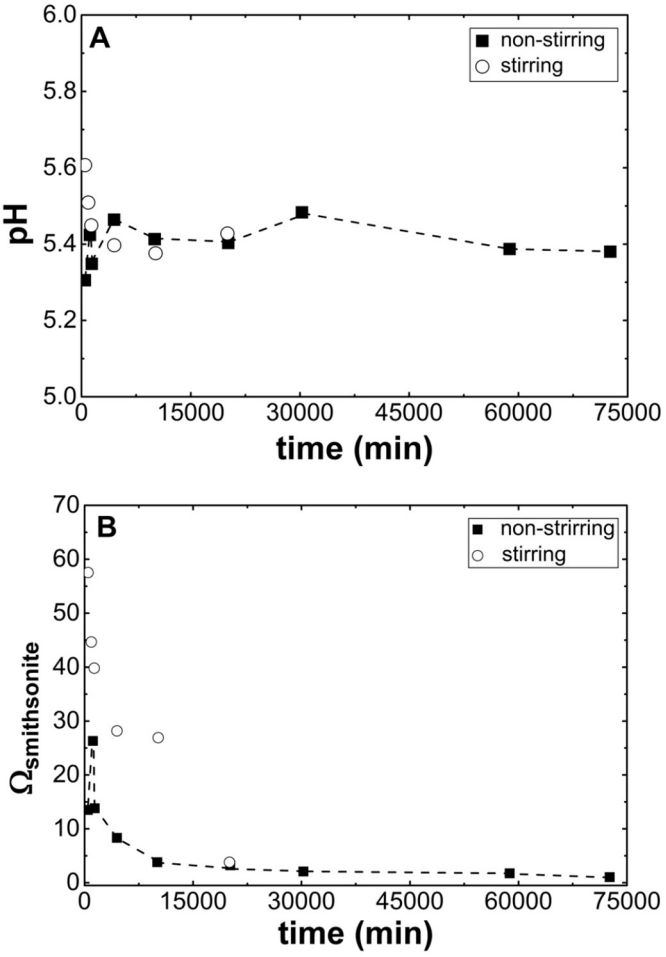

Fig. 4. (A) pH of precipitating solution as a function of reaction time at 25 °C in the stirring versus non-stirring reactor; and (B) Saturation degree in respect to smithsonite (at steady state Ωsmithsonite = 1.1 ± 0.3) plotted as a function of reaction time at 25 °C in the stirring versus non-stirring reactor. The curve was connected via two points by a single line.

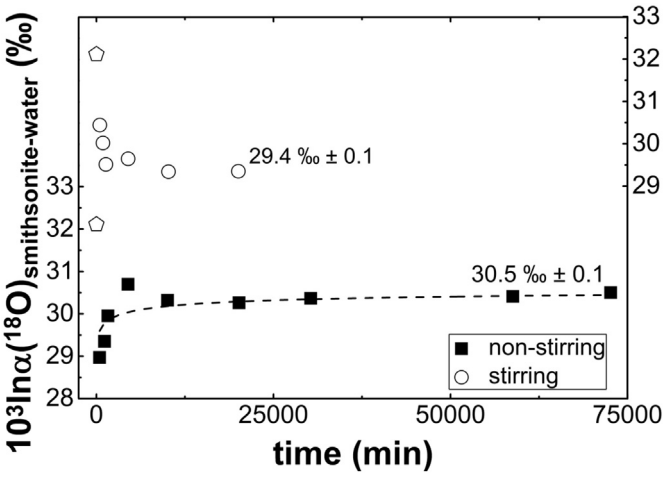

Fig. 5. Temporal evolution of the $10^3\ln\alpha(^{18}O)$smithsonite-water value for the oxygen isotope fractionation between the precipitate and water for experiments conducted at 25 °C as a function of reaction time in the stirring versus non-stirring reactor. The pentagon symbol represents the oxygen isotope fractionation of the precipitated hydrozincite (t = 0 min). The curves were fitted using a calculation of Origin: $10^3\ln\alpha_{\text{smithsonite-water}} = a - b * \log(c * \text{time}\ \ [\text{min}])$. Errors are with the size of the symbols.

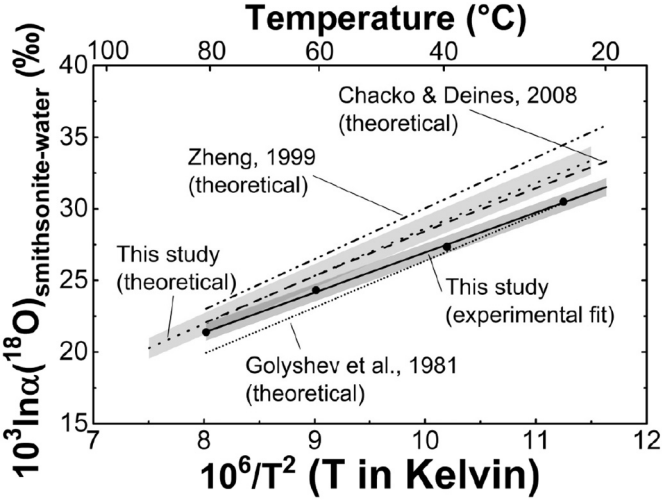

Fig. 6. Oxygen isotope fractionation between smithsonite and water as a function of temperature. Solid symbols represent the obtained data from this study for smithsonite formation in the non-stirring reactor (only isotope values between 25 °C and 80 °C for a reaction time ≥ 10,000 min are shown, where oxygen isotope fractionation is approaching equilibrium). Dashed line represents the theoretical calculation of Chacko and Deines (2008), dashed-dotted line of Zheng (1999), small dotted line of Golyshev et al. (1981) and the dotted line shows the ab-initio calculation (of the present study).

Table 2
Structural parameters of calcite and smithsonite, compared with experiment (exp.) and previous calculations (PBE). The numbers in parenthesis refer to uncertainties on the last significant digit.

	Calcite			Smithsonite		
	This work	Exp[a]	PBE[b]	This work	Exp[a]	PBE[c]
a (Å)	5.0600	4.9896[2]	5.0352	4.7207	4.6526[7]	4.714
c (Å)	17.2046	17.0610[11]	17.2194	15.3211	15.0257[22]	15.28
x(O)	0.25729	0.25682[11]		0.27550	0.27636[11]	

[a] Effenberger et al. (1981).
[b] Schauble et al. (2006).
[c] Ducher et al. (2016).

uncertainty on the obtained corrected law, resulting both from the uncertainty on the scaling factor and from the estimated 0.5‰ additional error discussed above, is also given on Table 4 and represented on Fig. A3. To obtain a mineral/liquid-water fractionation (calcite: Fig. A2; smithsonite: Fig. 6), we combined our calculated calcite/gas-water fractionation with the liquid/gas-water experimental fractionation determined by Horita and Wesolowski (1994). If we limit ourselves to the 0–100 °C temperature interval, these laws can be given as:

$$10^3\ln\alpha_{\text{calcite}-\text{liquid water}} = (2.65*10^6/T^2 - 4.87) \pm (0.025*10^6/T^2 + 0.90) \quad (6)$$

$$10^3\ln\alpha_{\text{smithsonite}-\text{liquid water}} = (3.21*10^6/T^2 - 3.63) \pm (0.025*10^6/T^2 + 0.90). \quad (7)$$

4. Discussion

4.1. Reaction mechanisms and pathways

Fig. 7 shows the individual stability fields of zincite, hydrozincite and smithsonite as a function of the partial pressure of CO_2 and pH according to the used thermodynamic data. At the beginning of each experiment hydrozincite is immediately precipitating at quasi neutral pH conditions (pH ~ 6.8) at 25 °C, and consistently the solution

Table 3
Comparison of model phonon frequencies in smithsonite and calcite with experimental data and other calculations (PBE). E_g and A_{1g} are Raman-active, A_{2u} and E_u are IR-active, A_{1u} and A_{2g} are silent modes. For IR-active modes, LO and TO frequencies are reported. For smithsonite, measurements (exp.) are from Frost et al. (2008a) for Raman, and Frost et al. (2008b) for infrared. For calcite, measurements (exp.) are from Gillet et al. (1993) for Raman, and from Hellwege et al. (1970), Cowley and Pant (1973), White (1974), and Gillet et al. (1996) for infrared.

Mode	Smithsonite			Calcite		
	This work	Exp	PBE	This work	Exp	PBE
E_g	177	196	178	152	156	151
	277	304	278	264	281	264
	693	730	697	680	711,709	689
	1342	1405–1409	1371	1372	1434	1392
A_{1g}	1047	1092	1063	1045	1086	1059
A_{2u}	139–231			114–142	92–132	112–140
	311–355			276–385	303–387	275–386
	810–827	(842),870	818	824–838	872–900	840–854
E_u	149			117–129	102–123	114–127
	183–222			205–216	223–239	205–216
	260–336			268–363	297–380	267–364
	705–707	(729),744		680–681	711	689–690
	1339–1496	(1335),1440	1369	1342–1486	1407–1549	1361–1506
A_{1u}	208			274		
	1047			1045		
A_{2g}	281			180		
	372			299		
	817			828		

Table 4
Fits of $10^3\ln\alpha(^{18}O)_{mineral\text{-}water(vapor)}$ for 0–400 °C, with x = 10^3/T. PBE refers to the uncorrected calculation. For the correction, see text. The estimated error on the corrected laws results from the propagation of the uncertainty on the scaling factor (1SE, see Appendix A) and from the 0.5‰ error (treated as an uncertainty) due to the neglect of anharmonicity for calcite and smithsonite (see text).

Mineral	Regression
Calcite (PBE)	$4.257–14.305x + 8.863 \times {}^{2}–0.656x^3$
Smithsonite (PBE)	$4.367–14.502x + 9.416x^2–0.7378x^3$
Calcite (corrected)	$3.9–13.8x + 9.42x^2–0.712x^3$
Smithsonite (corrected)	$4.0–14.0x + 10.02x^2–0.737x^3$
Error of corrected laws	$0.7 + 0.07x – 0.004x^2 + 9.10^{-5}x^3$

composition is plotting within the stability field of hydrozincite (Fig. 7). The increase of the pCO_2 pressure to about 10 atm results in a pH decrease. Accordingly, the solution composition shifts into the stability field of smithsonite at temperatures between 25 and 80 °C. Smithsonite is subsequently formed via dissolution of hydrozincite. For the final experimental solutions chemical equilibrium in respect to smithsonite solubility is reached (see saturation degrees in Table 1 and exemplarily shown for T = 25 °C; Fig. 4).

4.2. Kinetics versus isotope equilibrium conditions

In earlier studies it has been well established that deviation from isotopic equilibrium in carbonate systems may affect apparent $10^3\ln\alpha_{carbonate\_mineral\text{-}water}$ values (Mills and Urey, 1940; McConnaughey, 1989; Kim et al., 2006; Dietzel et al., 2009; Gabitov et al., 2012; Gabitov, 2013; Watkins et al., 2014). Due to the lack of oxygen isotopic equilibrium data for smithsonite precipitated in the laboratory, this study explores the temporal evolution of $\alpha_{smithsonite\text{-}water}$ at 25 °C, in order to verify the achievement of a constant oxygen isotopic fractionation between smithsonite and water as a function of reaction time (see Fig. 5).

As it can be seen in Fig. 5 $\alpha_{smithsonite\text{-}water}$ achieves quasi constant values that can be attributed to near isotopic equilibrium conditions. We note here that at a given reaction stage of the experiments kinetic effects might occur. These effects can be related to isotopic dis-equilibrium conditions among DIC species and/or high precipitation rates of carbonate minerals from solution, that can induce non-equilibrium isotopic conditions at the solid-liquid interface (e.g. Jiménez-López et al., 2001 for Mg-calcite; Dietzel et al., 2009 for calcite; Mavromatis

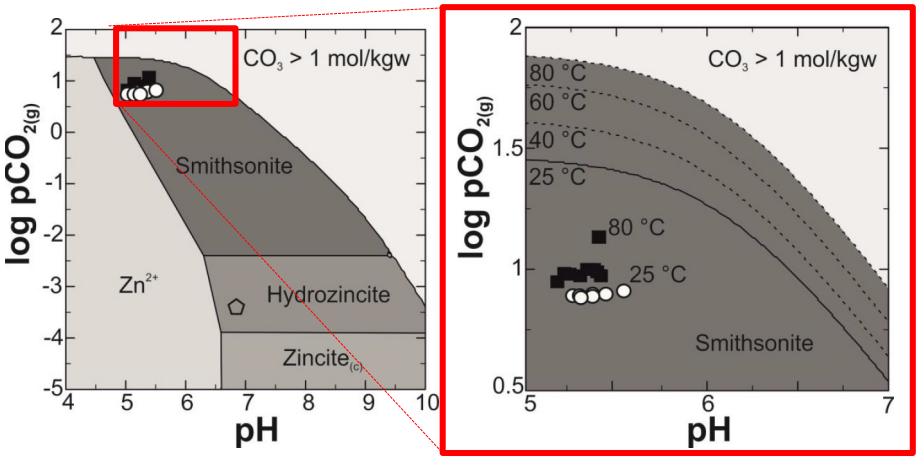

Fig. 7. Stability fields of zincite, hydrozincite versus smithsonite at 25 °C as a function of CO2 partial pressure (pCO2 in atm) and pH calculated using PHREEPLOT combined with PHREEQC software (see text for details). The pentagon symbol in the left diagram represents the initial experimental solution indicating hydrozincite formation as transition step at 25 °C and low pCO2. The enhanced detail on the right side shows the smithsonite stability field from 25, 40, 60 to 80 °C. The open circles (stirred experiments) and closed squares (non-stirred experiments) refer to the chemical composition and the CO_2 partial pressure shift of the experimental solutions for the temperature of 25 and 80 °C calculated with PhreeqC; 40 and 60 °C data points are lying in between those for 25 and 80 °C (this study).

et al., 2012 for Mg-calcite). In particular, the latter effect might be valid in this study for initial hydrozincite formation due to mixing of the two stock solutions inducing extremely high supersaturation of the resulting solution with respect to hydrozincite ($\Omega_{hydrozincite} = 10^{7.01}$; see Table 1). On the other hand the long term temporal evolution of the $\alpha_{smithsonite\text{-}water}$ value as it is depicted in Fig. 5, together with the increase in the average diameter of the formed crystal (Fig. 3B–F) rather suggest near equilibrium isotope exchange between smithsonite and the reactive fluid.

The temporal evolution of the oxygen isotope fractionation between smithsonite and water is divided into two parts. The first part (in the range from 465 to 1410 min) shows a contrasting behavior of the $10^3\ln\alpha_{smithsonite\text{-}water}$ values between the experiments using the non-stirring and stirring reactor (see Fig. 5 and discussion above). This contrasting behavior, in analogy to experiments with different agitation and shaking frequencies of Chacko et al. (1991) and Fortier (1994), might be caused by the continuous agitation of the solution in the experiments using the stirring reactor. The agitation of the solution might lead to a fast oxygen exchange rate between smithsonite and the CO_2 and follows a higher oxygen isotope fractionation.

In the second part (≥1410 min) of the experiments the evolution of $10^3\ln\alpha_{smithsonite\text{-}water}$ values using the non-stirring and stirring reactor shows a similar behavior. With increasing reaction time (≥10,000 min) $10^3\ln\alpha_{smithsonite\text{-}water}$ reached a constant value, suggesting near isotopic equilibrium conditions, at a similar reaction time, where isotope equilibrium between Mg-calcite and precipitating solution is reached (see Mavromatis et al., 2012; t ~14,400 min). Note here that the transformation of hydrozincite to smithsonite proceeds via a dissolution and re-precipitation process. Therefore isotopic memory effects from the precursor phase hydrozincite are unlikely to occur at the final stage of the experiments.

4.3. Oxygen isotope equilibrium fractionation between different metal carbonate minerals and water

In the present study experimental times of ≥10,000 min were used to study oxygen isotopic between smithsonite and solution at temperatures ranging from 25 to 80 °C at close isotopic equilibrium conditions (see discussion above; Fig. 6). The obtained decrease of $10^3\ln\alpha_{smithsonite\text{-}water}$ values with increasing temperature is a common feature when isotopic equilibrium is achieved also shown by other experimental studies, e.g. for calcite, aragonite, dolomite and siderite (e.g. McCrea, 1950; O'Neil et al., 1969; Tarutani et al., 1969; McConnaughey, 1989; Kim et al., 2006; Dietzel et al., 2009; Mavromatis et al., 2012; van Dijk et al., 2017), as well as in theoretical studies (Urey, 1947; Zheng, 1999; Watson, 2004; Schauble et al., 2006; Chacko and Deines, 2008; Zheng, 2011). In order to verify our experimental data in the scope of oxygen isotope fractionation between various carbonate minerals and water from other experimental studies Fig. 8 illustrates the respective $10^3\ln\alpha(^{18}O)$ values as a function of temperature. The most noticeable result for the oxygen isotope fractionation as a function of temperature is that all carbonate-water fractionation curves are positioned parallel to one another indicating different oxygen isotope fractionation up to several per mil between various carbonates (see also O'Neil et al. (1969) and Chacko et al. (2001)). The general finding is: the smaller the cation radius the higher the $10^3\ln\alpha(^{18}O)$ value. Chacko and Deines (2008) pointed out that both, the increase in cationic size and cationic mass, influence the preferentially incorporation of lighter oxygen isotopes in the carbonate mineral, based on internal vibrations of the carbonate and structure motions (e.g. O'Neil et al., 1969; Golyshev et al., 1981; Kim and O'Neil, 1997). Our experimental data fit into the obtained sequence of $Zn^{2+} < Fe^{2+} < Mn^{2+} < Ca^{2+}$ for mono-cation trigonal Me-carbonate minerals at isotopic equilibrium (Fig. 8).

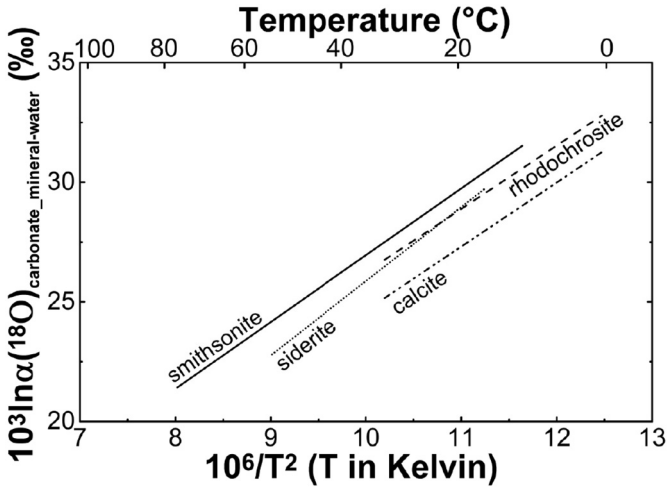

Fig. 8. Oxygen isotope fractionation between smithsonite and water (see Eq. (5)) as a function of temperature for those of mono-cation trigonal Me-carbonate minerals: siderite (van Dijk et al., 2017); rhodochrosite (Kim et al., 2009); calcite (Kim and O'Neil, 1997).

4.4. Ab initio calculations of smithsonite-water fractionation and comparison to experimental data

The corrected theoretical oxygen isotopic fractionation factor between calcite and water obtained in our study is in good agreement both with earlier theoretical calculations (i.e. Chacko and Deines, 2008) and with experimental data sets, at least in temperatures above 40 °C (Fig. A2 of the Appendix). This confirms the quality of Chacko and Deines (2008) calculations and underlines the use of this correction procedure.

The three computational ab initio models exhibit the general trend of decreasing oxygen isotope fractionation with increasing temperature such as with the experimental data (see Fig. 6). However, the existing theoretical data (e.g. Zheng, 1999; Chacko and Deines, 2008) as well as the data from the new ab initio calculation are slightly heavier compared to the measured oxygen isotopic fractionation factors of this study. As different simulation types of liquid water can be used for theoretical calculations, we assume that the discrepancy between the theoretical calculations (e.g. Zheng, 1999; Chacko and Deines, 2008 and this study) and the experimental data from this study may be explained by less precisely described anharmonicity of liquid water and/or not completely reaching isotopic equilibrium through kinetic effect in the experiments (see discussion above). Kinetic effects might be an additional cause for the deviation between experimental and calculated data.

4.5. Revisiting oxygen isotope fractionation between theoretical calculations and experimental data of various carbonates

In order to classify our experimental and theoretical data, in Fig. 9 oxygen isotope fractionation between various carbonate minerals and water is combined as a function of their ion radius at 25 °C. As it can be seen the $10^3\ln\alpha_{carbonate\_mineral\text{-}water}$ values of the experimental data are located above for Zn, Fe and Cd, underneath for Pb and Ba and on an equal level for Mn, Ca and Sr in comparison to the theoretical calculations of Chacko and Deines (2008).

The interesting finding is that the theoretical $10^3\ln\alpha_{carbonate\_mineral\text{-}water}$ values not completely follow the trend of decreasing oxygen isotope fractionation with increasing ionic radius. For instance, though the sequence of the ionic radius is $Fe^{2+} < Mn^{2+} < Cd^{2+}$ the theoretical $10^3\ln\alpha_{carbonate\_mineral\text{-}water}$ values are increasing. Furthermore, the sequence of the ionic radius is $Sr^{2+} < Pb^{2+} < Ba^{2+}$, certainly the theoretical $10^3\ln\alpha_{carbonate\_mineral\text{-}water}$ value of cerussite forms a

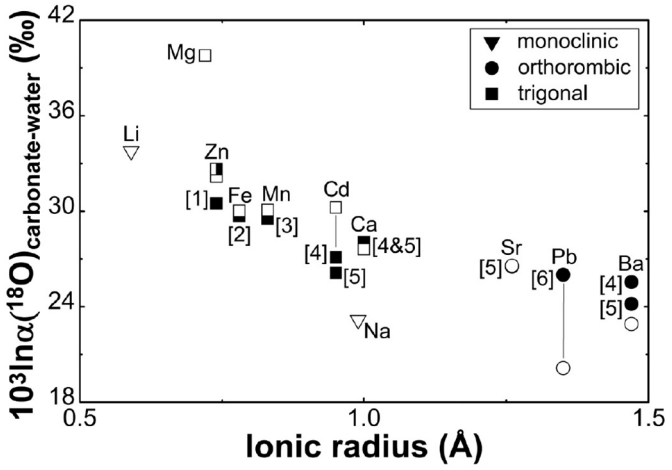

Fig. 9. Dependence of oxygen isotope fractionation between endmember metal carbonate minerals and water at 25 °C on the respective ionic metal radius. The data given in unfilled symbols are from the ab-initio calculation of Chacko and Deines (2008) and of this study in the half-filled symbol. The data from experimental studies are illustrated in filled symbols from [1] this study; [2] van Dijk et al. (2017); [3] Kim et al. (2009); [4] Kim and O'Neil (1997); [5] O'Neil et al. (1969); [6] Melchiorre et al. (2001).

downward peak between strontianite and witherite. In addition, the difference between theoretical and experimental $10^3 ln\alpha_{carbonate\_mineral\text{-}water}$ values is up to 4‰ for Cd and 6‰ for Pb. In contrast, our experimental data fit well into the experimental data of the literature following the finding: the smaller the cation radius the larger the oxygen isotope fractionation.

4.6. Implications for natural systems

The temperature-dependent oxygen isotope fractionation between carbonate minerals and water can act as a sensitive indicator for the temperature during their formation (Clayton and Epstein, 1961; O'Neil and Clayton, 1964). However, it has to be considered that the requirements and conditions to use the oxygen isotope fractionation between carbonate minerals and water as an environmental proxy are more complex in natural systems compared to experimental and theoretical studies due to (i) uncertainties in knowledge or estimation of the oxygen isotope composition of the precipitating solution (Gilg et al., 2008), (ii) use of proper mineral-water fractionation factors from literature (Boni et al., 2003; Boni et al., 2007; Gilg et al., 2008; this study), and (iii) unknown and/or varying physicochemical conditions during carbonate formation, such as pH, salinity, CO_2 pressure, which can affect the apparent $\alpha_{carbonate\_mineral\text{-}water}$ values e.g. due to kinetic effects.

In natural surroundings smithsonite formation is mostly related to oxidation of Zn containing solid sulfide phases by water circulation, e.g. in a deep karstic network (Alwan and Williams, 1979; Williams, 1990; Anthony et al., 2003; Boni et al., 2003) as well as in mines and deposits in Sardinia (Boni et al., 2003), in the Irish midlands (Boni et al., 2007) and in Belgium (Coppola et al., 2008). Thus from another point of view unravelling smithsonite formation conditions may open up new insights into secondary events, which have overprinted the primary depositing mineral association. In particular geological and environmental events, which create elevated pCO_2, can be recognized and studied by smithsonite formation via decomposition of initially formed hydrozincite.

For instance, in 2003, Boni et al. measured oxygen isotopes of different smithsonite types from the deposits of the Iglesias Valley in the southwest of Sardinia, which are dominated by Paleozoic rocks of sedimentary and igneous origin. They measured $\delta^{18}O$ values for smithsonite of 27.4 ± 0.9‰ (given in VSMOW). In order to calculate the smithsonite formation temperature they used the equation of Zheng (1999) and the estimated $\delta^{18}O$ values of De Vivo et al. (1987) for the forming water between −7.0 and −4.5‰ (VSMOW). Hence, they calculated a formation temperature ranging between 20 and 35 °C. However, using the Eq. (5) based on our experimental data the formation temperature is ranging between 10 and 20 °C. As the experimental approach results in most reliable temperature-dependent oxygen isotope fractionation between smithsonite and water (see discussion above), we assume that the latter lower temperature range to be valid, which is also closer to the average air temperature in the area.

Calculation of the smithsonite formation temperature from natural samples in future studies should include the use of clumped isotopes analyses for naturally formed smithsonite in order to precisely determine the temperatures of mineral formation or overprinting/diagenetic event. Subsequently the oxygen isotopic composition of the reacting fluid can be obtained by Eq. (5). Secondly, an advanced approach for studying multi metal carbonate (Me) containing deposits is suggested based on the distinct oxygen isotope signatures of the above mono-cation trigonal Me-carbonate minerals to follow the variability and sequences of post depositional changes in environmental settings. For this purpose e.g. siderite might be of special interest as it forms exclusively at reducing conditions (Boni et al., 2003; Coppola et al., 2008). As it can be seen in Fig. 8, the regression line for siderite shows a different slope compared to smithsonite. Therefore, the difference in the oxygen isotope fractionation ($\Delta^{18}O_{siderite\text{-}smithsonite} = \delta^{18}O_{siderite} - \delta^{18}O_{smithsonite}$) according to the expression

$$\Delta^{18}O_{siderite-smithsonite} = 0.31 * 10^6/T^2 - 4.15 \quad (8)$$

may provide an interesting tool for the determination of carbonate minerals formation temperatures if close to isotopic equilibrium conditions and the identical precipitating fluid can be reasonably assumed, in particular for elevated temperatures (e.g. $\Delta^{18}O_{siderite\text{-}smithsonite} = -1.66$‰ at 80 °C).

5. Summary and conclusions

In the present study first experimental results on the oxygen isotope fractionation between smithsonite and water are presented to study the, until now, poorly constrained $\alpha_{smithsonite\text{-}water}$ and its temperature dependence. Therefore, the formation of smithsonite was induced by the transformation of hydrozincite between 25 and 80 °C. The main conclusions of the experimental and modeling results are as follows:

(1) The temporal evolution of the oxygen isotope fractionation between smithsonite and water indicates the achievement of close to isotopic equilibrium conditions at a reaction time of about 10,000 min (~7 days) at $T \geq 25$ °C, independent from the hydrodynamic flow/mixing conditions of the experiments.
(2) The oxygen isotope fractionation between smithsonite and water at isotopic equilibrium can be calculated as a function of temperature from 25 to 80 °C according to expression (5) based on the experimental data.
(3) The $\alpha(^{18}O)_{smithsonite\text{-}water}$ values from the experimental approach fit within error to the theoretical relationship from the literature and our ab initio calculations. Discrepancies can be explained by the non-precisely described anharmonicity of water and/or by non-entirely approaching isotopic equilibrium throughout formation of smithsonite.
(4) The transformation of hydrozincite, likely forming in sulfide deposits, to smithsonite throughout exposure to solutions at elevated pCO_2 is caused by dissolution and re-crystallization reactions. This reaction paths/mechanisms and its oxygen isotope fractionation behavior can be assessed to evaluate environmental and post-depositional environmental conditions of zinc-bearing sedimentary ores.

Acknowledgements

The research was financially supported by the Marie Skłodowska-Curie Horizon 2020 project BASE-LiNE Earth (H2020-MSCA-INT-2014-643084) and the FWF-DFG project Charon II (FWF I3028-N29). Ab initio calculations were performed using HPC resources from CALMIP (Grant 2017-p1037). We are thankful to A. Geisinger-Haslinger, S. Lindbichler and B. Zirngast for measuring oxygen isotope ratios of the aqueous solutions as well as A. Baldermann and S. Eichinger for measuring element concentrations by ICP-OES. The manuscript benefited from thoughtful comments by I. Kell-Duivestein. Two anonymous reviewers and Editor-in-Chief, Michael E. Böttcher, are highly acknowledged for their insightful comments on a previous version of this manuscript.

Appendix A. 1/ Frequency scaling procedure to correct the carbonate-vapor fractionation factor

For calcite, a good agreement is observed between calculated frequencies and experimental ones (Table 3). Generally, the calculated frequencies underestimate experiment by a few %, but the relative error is varying depending on the modes.

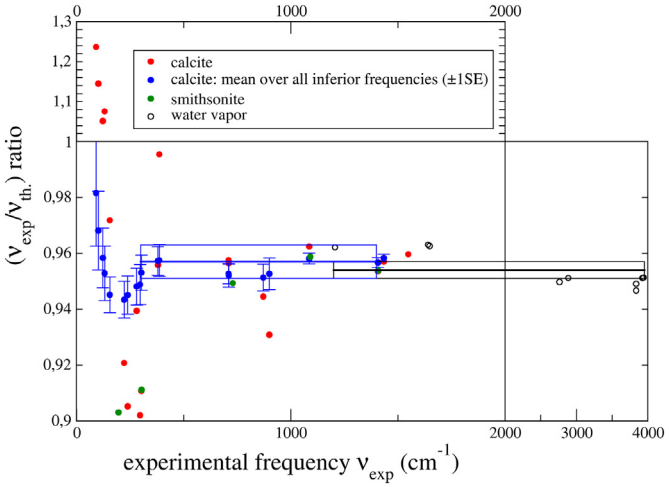

Fig. A1. Ratio between calculated frequencies and their experimental counterpart. Red and green plain circles are the ratios of each mode taken from Table 3, for calcite and smithsonite, respectively. Blue symbols are averages of the ratios of calcite over all the modes with frequencies equal or lower than the corresponding experimental frequency. The chosen values for the correction procedure are the blue line (0.957 ± 0.006), for calcite and smithsonite, and the black line (0.954 ± 0.003) for the water molecule (see text for details). (For interpretation of the references to colour in this figure legend, the reader is referred to the web version of this article.)

As can be seen on Fig. A1, the four lowest frequencies of calcite (around 100–150 cm^{-1}) are significantly overestimated, on the contrary to the rest, and for the above frequencies up to about 300 cm^{-1}, the ratio is varying significantly. Looking at the average ratio, we find 0.982 ± 0.019 (1SE) if we consider all the modes, but 0.957 ± 0.006 (1SE) if we consider only the frequencies higher than 350 cm^{-1}. Since the low frequency modes are not expected to strongly impact fractionation, we will choose this value of 0.957 ± 0.006 (blue box on Fig. A1) to discuss the consequences of this error on the fractionation properties. Also, Fig. A1 suggests no difference between the frequency ratio of calcite and of smithsonite. This is consistent with Schauble et al., 2006 who concluded on the adequacy of a unique scale factor for several anhydrous carbonate minerals.

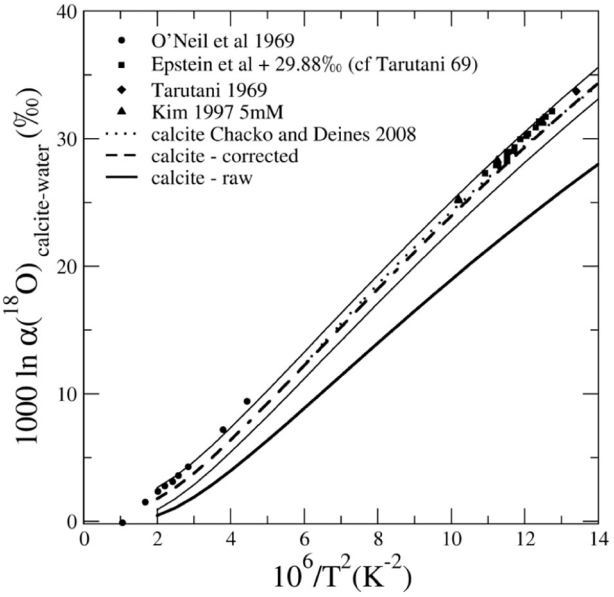

Fig. A2. Oxygen isotope fractionation between calcite and fluid as a function of temperature (this study) compared to previous studies. The two thin plain lines framing the corrected law correspond to the estimated error of this corrected calculation (see text).

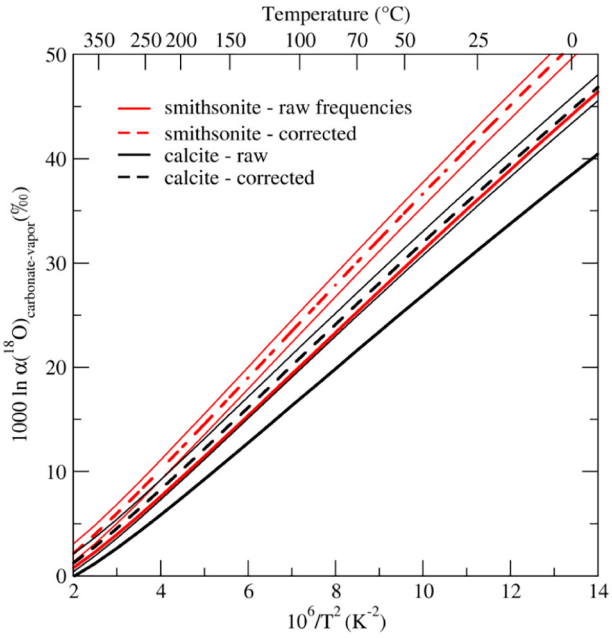

Fig. A3. Calculated fractionation factors between carbonates and an isolated water molecule. Plain line: obtained with the harmonic frequencies calculated from ab initio methods. Dashed line: fractionation factors corrected and their associated error (see text).

The mineral-water vapor fractionation factors, calculated directly from these ab initio-based harmonic frequencies, are shown as a function of temperature on Fig. A3. To correct for the approximations inherent to our methodology, we realized two corrections. First, to correct for the error on harmonic frequencies, we rescaled them. For calcite and smithsonite, the scaling factor considered was 0.957 ± 0.006. For water vapor, based on our previous calculation (see Table 2 of Méheut et al., 2007), we obtain a mean scaling factor of 0.954 ± 0.003 (1SE). Second, to correct for anharmonicity, we added the anharmonic contribution determined by Richet et al. (1977). To obtain a calcite-water law, we combined the calcite-vapor calculation with the experimental liquid-vapor law proposed by Horita and Wesolowski (1994) (Fig. A3). For calcite, the corrected law is in good agreement with both experimental data and previous theoretical studies.

Table A4
Temperature, pH, pCO_2, alkalinity, duration, added $NaHCO_3$ and $Zn(NO_3)_2$, final $NaHCO_3$ and $Zn(NO_3)_2$ of the experimental solution. $\delta^{18}O$ values of the precipitates and water relative to *V*ienna Standard Mean Ocean Water (VSMOW). $10^3 ln\alpha(^{18}O)_{precipitate–water}$: Oxygen isotopic fractionation between the precipitate and water.

No.	T (°C)	pH	Alkalinity (mmol/L)	pCO_2 (atm)	t (min)	Added $NaHCO_3$ (mM)	Added Zn $(NO_3)_2$ (mM)	Final $NaHCO_3$ (mM)	final Zn $(NO_3)_2$ (mM)	$\delta^{18}O$ precipitate	$\delta^{18}O_{water}$	$10^3 ln\alpha(^{18}O)$ precipitate-water	$\Omega_{precipitate}$
Precursor phase (hydrozincite)													
T25_0[a]	25	6.83	70.0	$10^{-3.4}$	0	199.8	40.94	189.9	5.22	22.75	−9.57	32.11	$10^{7.01}$
Smithsonite (non-stirring)													
T25_1.1	25	5.31	38.6	9.3	465	228.7	43.5	138.4	2.70	19.43	−9.68	28.97	13.49
T25_1.2	25	5.42	51.9	9.5	1160	199.5	44.2	118.9	3.53	20.11	−9.69	29.64	26.30
T25_1.3	25	5.35	42.8	9.5	1410	249.5	43.2	108.2	2.39	20.49	−9.62	29.95	13.80
T25_1.4	25	5.46	56.0	9.8	4485	199.6	42.1	107.0	0.97	21.24	−9.63	30.69	8.32
T25_1.5	25	5.41	49.3	9.3	10,050	201.4	42.8	117.0	0.53	20.77	−9.72	30.32	3.80
T25_1.6	25	5.40	48.0	9.5	20,150	199.4	43.2	118.9	0.47	20.74	−9.68	30.26	3.24
T25_1.7	25	5.48	58.5	9.3	30,270	202.0	42.8	201.2	0.23	20.87	−9.66	30.36	2.09
T25_1.8	25	5.39	46.1	9.8	58,790	201.2	43.0	101.8	0.27	21.05	−9.53	30.41	1.74
T25_1.9	25	5.38	38.0	9.9	72,620	207.7	44.2	97.2	0.21	21.06	−9.61	30.50	1.05
T40_1	40	5.32	30.9	9.5	24,240	98.1	21.8	140.8	0.48	17.93	−9.53	27.35	3.89
T40_2	40	5.54	54.3	10	4125	199.8	39.1	109.6	0.40	18.09	−9.31	27.28	6.17
T60_1	60	5.50	37.6	10.5	18,815	100.2	20.0	163.4	0.33	14.41	−9.43	23.79	7.24
T60_2	60	5.06	13.0	11	26,930	103.0	21.1	61.6	0.43	14.23	−10.14	24.32	2.14
T80	80	5.48	29.1	12.9	10,035	100.0	21.0	81.9	0.36	12.22	−9.19	21.38	10.96
Smithsonite (stirring)													
T25s_1.1	25	5.61	81.6	9.3	490	226.4	36.9	201.3	4.40	21.06	−9.55	30.44	57.54
T25s_1.2	25	5.51	64.4	9.1	930	188.5	39.8	200.6	4.56	20.6	−9.58	30.02	44.67
T25s_1.3	25	5.45	55.8	9.1	1345	170.1	39.8	204.5	4.94	19.99	−9.67	29.51	39.81

(*continued on next page*)

Table A4 (*continued*)

No.	T (°C)	pH	Alkalinity (mmol/L)	pCO_2 (atm)	t (min)	Added $NaHCO_3$ (mM)	Added Zn $(NO_3)_2$ (mM)	Final $NaHCO_3$ (mM)	final Zn $(NO_3)_2$ (mM)	$\delta^{18}O$ precipitate	$\delta^{18}O_{water}$	$10^3 ln\alpha(^{18}O)$ precipitate-water	$\Omega_{precipitate}$
T25s_1.4	25	5.40	48.9	8.9	4490	179.0	38.5	197.7	4.12	20.14	−9.66	29.64	28.18
T25s_1.5	25	5.38	46.5	8.9	10,170	166.4	39.5	202.4	4.25	19.87	−9.62	29.34	26.92
T25s_1.6	25	5.43	51.1	9.1	20,040	202.1	39.9	111.6	0.50	19.84	−9.66	29.35	3.80

s = precipitation of smithsonite by using a stirred reactor.

[a] Hydrozincite precipitated at the initial stage of the experiments at 25 °C.

References

Alwan, A.K., Williams, P.A., 1979. Transition Metal Chemistry, 4th ed. Netherlands, Dordrecht.

Anthony, J.W., Bideaux, R.A., Bladh, K.W., Nichols, M.C., 2003. Handbook of Mineralogy. Mineral Data Publishing, Tiscon, AZ, USA.

Baroni, S., de Gironcoli, S., Dal, Corso A., Giannozzi, P., 2001. Phonons and related crystal properties from density-functional perturbation theory. Rev. Mod. Phys. 73.

Beck, W.C., Grossman, E.L., Morse, J.W., 2005. Experimental studies of oxygen isotope fractionation in the carbonic acid system at 15°, 25°, and 40 °C. Geochim. Cosmochim. Acta 69, 3493–3503.

Becker, R.H., Clayton, R.N., 1976. Oxygen isotope study of a Precambrian banded iron-formation, Hamerslay Range, Western Australia. Geochim. Cosmochim. Acta 40, 1153–1165.

Bigeleisen, J., Mayer, M.G., 1947. Calculation of equilibrium constants for isotopic exchange reactions. J. Chem. Phys. 15, 261–267.

Boni, M., Gilg, H.A., Aversa, G., Balassone, G., 2003. The "Calamine" of southwest Sardinia: geology, mineralogy, and stable isotope geochemistry of supergene Zn mineralization. Econ. Geol. 98, 731–748.

Boni, M., Balassone, G., Gilg, H.A., Stanley, G., 2007. Non-sulphide Zn-Pb mineralization in the Irish Midlands (Tynagh, Silvermines and Galmoy). In: Digging Deep, pp. 1377–1380.

Bouchard, M., Smith, D.C., 2001. Evaluating Raman microscopy for the non-destructive archaeometry of corroded coins: a powerful technique for conservation studies. Invited paper. Asian Chem. Lett. 5, 157–170.

Carothers, W.W., Adami, L.H., Rosenbauer, R.J., 1988. Experimental oxygen isotope fractionation between siderite-water and phosphoric-acid liberated CO_2-siderite. Geochim. Cosmochim. Acta 52, 2445–2450.

Chacko, T., Deines, P., 2008. Theoretical calculation of oxygen isotope fractionation factors in carbonate systems. Geochim. Cosmochim. Acta 72, 3642–3660.

Chacko, T., Mayeda, T.K., Clayton, R.N., Goldsmith, J.R., 1991. Oxygen and carbon isotope fractionations between CO_2 and calcite. Geochim. Cosmochim. Acta 55, 2867–2882.

Chacko, T., Cole, D.R., Horita, J., 2001. Equilibrium oxygen, hydrogen and carbon isotope fractionation factors applicable to geologic systems. In: Stable Isotope Geochemistry, pp. 1–81.

Clayton, R.N., Epstein, S., 1961. The use of oxygen isotopes in high-temperature geological thermometry. J. Geol. 69, 447–452.

Coplen, T.B., Kendall, C., Hopple, J., 1983. Comparison of stable isotope reference samples. Nature 302, 236–238.

Coppola, V., Boni, M., Gilg, H.A., Balassone, G., Dejonghe, L., 2008. The "calamine" nonsulfide Zn-Pb deposits of Belgium: petrographical, mineralogical and geochemical characterization. Ore Geol. Rev. 33, 187–210.

Cowley, E.R., Pant, A.K., 1973. Lattice dynamics of calcite. Phys. Rev. B 8, 4795–4800.

Dal, Corso A., 2014. Pseudopotentials periodic table: from H to Pu. Comput. Mater. Sci. 95, 337–350.

De Vivo, B., Maiorani, A., Perna, G., Turi, B., 1987. Fluid inclusion and stable isotope studies of calcite, quartz and barite from karstic caves in the Masua mine, southwestern Sardinia, Italy. Chem. Erde 46, 259–273.

Deines, P., 2004. Carbon isotope effects in carbonate systems. Geochim. Cosmochim. Acta 68, 2659–2679.

Dietzel, M., Tang, J., Leis, A., Köhler, S.J., 2009. Oxygen isotopic fractionation during inorganic calcite precipitation - effects of temperature, precipitation rate and pH. Chem. Geol. 268, 107–115.

Ducher, M., Blanchard, M., Balan, E., 2016. Equilibrium zinc isotope fractionation in Zn-bearing minerals from first-principles calculations. Chem. Geol. 443, 87–96.

Effenberger, H., Mereiter, K., Zemann, J., 1981. Crystal structure refinements of magnesite, calcite, rhodochrosite, siderite, smithsonite, and dolomite, with discussion of some aspects of the stereochemistry of calcite type carbonates. Z. Krist. 156, 233–243.

Epstein, S., Mayeda, T., 1953. Variation of O^{18} content of waters from natural sources. Geochim. Cosmochim. Acta 4, 213–224.

Farmer, V.C., 1974. The Infrared Spectra of Minerals. Mineralogical Society.

Fortier, S.M., 1994. An on-line experimental/analytical method for measuring the kinetics of oxygen isotope exchange between CO_2 and saline/hypersaline salt solutions at low (25–50°C) temperatures. Chem. Geol. 116, 155–162.

Frost, R.L., Hales, M.C., Wain, D.L., 2008a. Raman spectroscopy of smithsonite. J. Raman Spectrosc. 39, 108–114.

Frost, R.L., Martens, W.N., Wain, D.L., Hales, M.C., 2008b. Infrared and infrared emission spectroscopy of the zinc carbonate mineral smithsonite. Spectrochim. Acta A Mol. Biomol. Spectrosc. 70, 1120–1126.

Gabitov, R.I., 2013. Growth-rate induced disequilibrium of oxygen isotopes in aragonite: an in situ study. Chem. Geol. 351, 268–275.

Gabitov, R.I., Watson, E.B., Sadekov, A., 2012. Oxygen isotope fractionation between calcite and fluid as a function of growth rate and temperature: an in situ study. Chem. Geol. 306, 92–102.

Giannozzi, P., Baroni, S., Bonini, N., Calandra, M., Car, R., Cavazzoni, C., Ceresoli, D., Chiarotti, G.L., Cococcioni, M., Dabo, I., Dal, Corso A., de Gironcoli, S., Fabris, S., Fratesi, G., Gebauer, R., Gerstmann, U., Gougoussis, C., Kokalj, A., Lazzeri, M., Martin-Samos, L., Marzari, N., Mauri, F., Mazzarello, R., Paolini, S., Pasquarello, A., Paulatto, L., Sbraccia, C., Scandolo, S., Sclauzero, G., Seitsonen, C., Smogunov, A., Umari, P., Wentzcovitch, R.M., 2009. QUANTUM ESPRESSO: a modular and open-source software project for quantum simulations of materials. J. Phys. Condens. Matter 21, 1–19.

Gilg, H.A., Struck, U., Vennemann, T., Boni, M., 2003. Phosphoric acid fractionation factors for smithsonite and cerussite between 25 and 72 °C. Geochim. Cosmochim. Acta 67, 4049–4055.

Gilg, H.A., Boni, M., Hochleitner, R., Struck, U., 2008. Stable isotope geochemistry of carbonate minerals in supergene oxidation zones of Zn-Pb deposits. Ore Geol. Rev. 33, 117–133.

Gillet, P., Biellmann, C., Reynard, B., McMillan, P., 1993. Raman spectroscopic studies of carbonates part I: high-pressure and high-temperature behaviour of calcite, magnesite, dolomite and aragonite. Phys. Chem. Miner. 20, 1–18.

Gillet, P., Mcmillan, P., Schott, J., Badro, J., Grzechnik, A., 1996. Thermodynamic properties and isotopic fractionation of calcite from vibrational spectroscopy of ^{18}O-substituted calcite. Geochim. Cosmochim. Acta 60, 3471–3485.

Golyshev, S.I., Padalko, N.L., Pechenkin, S.A., 1981. Fractionation of stable oxygen and carbon isotopes in carbonate systems. Geochem. Int. 18, 85–99.

Hales, M.C., Frost, R.L., 2007. Synthesis and vibrational spectroscopic characterisation of synthetic hydrozincite and smithsonite. Polyhedron 26, 4955–4962.

Hellwege, K.H., Lesch, W., Plihal, M., Schaack, G., 1970. Two phonon absorption spectra and dispersion of phonon branches in crystals of calcite structure. Z. Phys. A: Hadrons Nucl. 232, 61–86.

Hoefs, J., 2015. Stable Isotope Geochemistry, 7th ed. Springer-Verlag, Heidelberg, Berlin.

Hohenberg, P., Kohn, W., 1964. Inhomogeneous electron gas. Phys. Rev. 136, 864–871.

Horita, J., Wesolowski, D.J., 1994. Liquid-vapor Fractionation of Oxygen and Hydrogen Isotopes of Water from the Freezing to the Critical Temperature. 58. pp. 3425–3437.

Horita, J., Ueda, A., Mizukami, K., Takatori, I., 1989. Automatic δD and $\delta^{18}O$ analyses of multi-water samples using H_2- and CO_2-water equilibration methods with a common equilibration set-up. Int. J. Rad. Appl. Instrum. 40, 801–805.

Jambor, J.L., 1964. Studies of basic copper and zinc carbonates: 1-synthetic zinc carbonates and their relationship to hydrozincite. In: Cabadian Mineral, pp. 92–108.

Jiménez-López, C., Caballero, E., Huertas, F.J., Romanek, C.S., 2001. Chemical, mineralogical and isotope behavior, and phase transformation during the precipitation of calcium carbonate minerals from intermediate ionic solution at 25 °C. Geochim. Cosmochim. Acta 65, 3219–3231.

Kim, S.T., O'Neil, J.R., 1997. Equilibrium and nonequilibrium oxygen isotope effects in synthetic carbonates. Geochim. Cosmochim. Acta 61, 3461–3475.

Kim, S.T., Hillaire-Marcel, C., Mucci, A., 2006. Mechanisms of equilibrium and kinetic oxygen isotope effects in synthetic aragonite at 25 °C. Geochim. Cosmochim. Acta 70, 5790–5801.

Kim, S.T., Kang, J.O., Seong-Taek, Y., O'Neil, J.R., Mucci, A., 2009. Experimental studies of oxygen isotope fractionation between rhodochrosite ($MnCO_3$) and water at low temperatures. Geochim. Cosmochim. Acta 73, 4400–4408.

Kim, S.T., Coplen, T.B., Horita, J., 2015. Normalization of stable isotope data for carbonate minerals: implementation of IUPAC guidelines. Geochim. Cosmochim. Acta 158, 276–289.

Kinniburgh, D.G., Cooper, D.M., 2011. PhreePlot: Creating Graphical Output with PhreeqC.

Kohn, W., Sham, L.J., 1965. Self-consistent equations including exchange and correlation effects. Phys. Rev. 140, 1133–1138.

Mavromatis, V., Schmidt, M., Botz, R., Comas-Bru, L., Oelkers, E.H., 2012. Experimental quantification of the effect of Mg on calcite-aqueous fluid oxygen isotope fractionation. Chem. Geol. 310–311, 97–105.

McConnaughey, T., 1989. ^{13}C and ^{18}O isotopic disequilibrium in biological carbonates: II. In vitro simulation of kinetic isotope effects. Geochim. Cosmochim. Acta 53,

163–171.
McCrea, J.M., 1950. On the isotopic chemistry of carbonates and a paleotemperature scale. J. Chem. Phys. 18, 849–857.
Méheut, M., Lazzeri, M., Balan, E., Mauri, F., 2007. Equilibrium isotopic fractionation in the kaolinite, quartz, water system: prediction from first-principles density-functional theory. Geochim. Cosmochim. Acta 71, 3170–3181.
Melchiorre, E.B., Williams, P.A., Bevins, R.E., 2001. A low temperature oxygen isotope thermometer for cerussite, with applications at Broken Hill, New South Wales, Australia. Geochim. Cosmochim. Acta 65, 2527–2533.
Mills, G.A., Urey, H.C., 1940. The kinetics of isotopic exchange between carbon dioxide, bicarbonate ion, carbonate ion and water. J. Am. Chem. Soc. 62, 1019–1026.
Monkhorst, H.J., Pack, J.D., 1976. Special points for Brillouin-zone integrations. Phys. Rev. B 13, 5188–5192.
O'Neil, J.R., Clayton, R.N., 1964. Oxygen isotope geothermometry. Isot. Cosm. Chem. 157–168.
O'Neil, J.R., Clayton, R.N., Toshiko, M.K., 1969. Oxygen isotope fractionation in divalent metal carbonates. J. Chem. Phys. 51, 5547–5558.
Parkhurst, D.L., Appelo, C.A.J., 1999. User's Guide to PHREEQC-A Computer Program for Speciation, Batch-Reaction, One-dimensional Transport, and Inverse Geochemical Calculations.
Paul, D., Skrzypek, G., 2007. Assessment of carbonate-phosphoric acid analytical technique performed using GasBench II in continuous flow isotope ratio mass spectrometry. Int. J. Mass Spectrom. 262, 180–186.
Perdew, J.P., Burke, K., Ernzerhof, M., 1996. Generalized gradient approximation made simple. Phys. Rev. 77, 3865–3868.
Polyakov, V.B., 1998. On anharmonic and pressure corrections to the equilibrium isotopic constants for minerals. Geochim. Cosmochim. Acta 62, 3077–3085.
Révész, K.M., Landwehr, J.M., 2002. $\delta^{13}C$ and $\delta^{18}O$ isotopic composition of $CaCO_3$ measured by continuous flow isotope ratio mass spectrometry: statistical evaluation and verification by application to Devils Hole core DH-11 calcite. Rapid Commun. Mass Spectrom. 16, 2102–2114.
Richet, P., Bottinga, Y., Javoy, M., 1977. A review of hydrogen, carbon, nitrogen, oxygen, sulphur, and chlorine stable isotope fractionation among gaseous molecules. Annu. Rev. Earth Planet. Sci. 5, 65–110.
Rosenbaum, J.M., 1997. Gaseous, liquid, and supercritical fluid H_2O and CO_2: oxygen isotope fractionation behavior. Geochim. Cosmochim. Acta 61, 4993–5003.
Schauble, E.A., Ghosh, P., Eiler, J.M., 2006. Preferential formation of ^{13}C-^{18}O bonds in carbonate minerals, estimated using first-principles lattice dynamics. Geochim. Cosmochim. Acta 70, 2510–2529.
Schindler, P., Reinert, M., Gamsjäger, H., 1969. Löslichkeitskonstanten und Freie Bildungsenthalpien von $ZnCO_3$ und $Zn_5(OH)_6(CO_3)_2$ bei 25°. Helv. Chim. Acta 52, 2327–2332.
Schmidt, M., Xeflide, S., Botz, R., Mann, S., 2005. Oxygen isotope fractionation during synthesis of CaMg-carbonate and implications for sedimentary dolomite formation. Geochim. Cosmochim. Acta 69, 4665–4674.
Spötl, C., Vennemann, T.W., 2003. Continuous-flow isotope ratio mass spectrometric analysis of carbonate minerals. Rapid Commun. Mass Spectrom. 17, 1004–1006.
Stoilova, D., Koleva, V., Vassileva, V., 2002. Infrared study of some synthetic phases of malachite ($Cu_2(OH)_2CO_3$)-hydrozincite ($Zn_5(OH)_6(CO_3)_2$) series. Spectrochim. Acta A Mol. Biomol. Spectrosc. 58, 2051–2059.
Tarutani, T., Clayton, R.N., Mayeda, T.K., 1969. The effect of polymorphism and magnesium substitution on oxygen isotope fractionation between calcium carbonate and water. Geochim. Cosmochim. Acta 33, 987–996.
Urey, H.C., 1947. The thermodynumic properties of isotopic substances. J. Chem. Soc. 562–581.
van Dijk, J., Fernandez, A., Müller, I.A., Lever, M., Bernasconi, S.M., 2017. Oxygen isotope fractionation in the siderite-water system between 8.5 and 62 °C. Geochim. Cosmochim. Acta 220, 535–551.
Wahab, R., Ansari, S.G., Kim, Y.S., Dar, M.A., Shin, H.S., 2008. Synthesis and characterization of hydrozincite and its conversion into zinc oxide nanoparticles. J. Alloys Compd. 461, 66–71.
Watkins, J.M., Hunt, J.D., Ryerson, F.J., Depaolo, D.J., 2014. The influence of temperature, pH, and growth rate on the $\delta^{18}O$ composition of inorganically precipitated calcite. Earth Planet. Sci. Lett. 404, 332–343.
Watson, E.B., 2004. A conceptual model for near-surface kinetic controls on the trace-element and stable isotope composition of abiogenic calcite crystals. Geochim. Cosmochim. Acta 68, 1473–1488.
White, W.B., Farmer, V.C., 1974. The carbonates minerals. In: The Infrared Spectra of Minerals, pp. 227–284 London.
Williams, P.A., 1990. Oxide Zone Geochemistry. Ellis Horwood Ltd., Chichester, West Sussex, England.
Zheng, Y.-F., 1999. Oxygen isotope in carbonate fractionation and sulfate minerals. Geochem. J. 33, 109–126.
Zheng, Y.-F., 2011. On the theoretical calculations of oxygen isotope fractionation factors for carbonate-water systems. Geochem. J. 45, 341–354.
Zhou, G.-T., Zheng, Y.-F., 2002. Kinetic mechanism of oxygen isotope disequilibrium in precipitated witherite and aragonite at low temperatures: an experimental study. Geochim. Cosmochim. Acta 66, 63–71.
Zhou, G.-T., Zheng, Y.-F., 2003. An experimental study of oxygen isotope fractionation between inorganically precipitated aragonite and water at low temperatures. Geochim. Cosmochim. Acta 67, 387–399.
Zhu, F., Persson, D., Thierry, D., 2001. Formation of corrosion products on open and confined metal surfaces exposed to periodic wet/dry conditions—a comparison between zinc and electrogalvanized steel. Corrosion 57, 582–590.